# Classification of Melanoma Lesions Using Sparse Coded Features and Random Forests

Mojdeh Rastgoo[a,b] and Guillaume Lemaître[a,b] and Olivier Morel[a] and Johan Massich[a] and Frank Marzani[a] and Rafael Garcia[b] and Désiré Sidibé[a]

[a]LE2I UMR6306, CNRS, Arts et Métiers, Univ. Bourgogne Franche-Comté, 12 rue de la Fonderie, 71200 Le Creusot, France;

[b]ViCOROB, Universitat de Girona, Campus Montilivi, Edifici P4, 17071 Girona, Spain

## ABSTRACT

Malignant melanoma is the most dangerous type of skin cancer, yet it is the most treatable kind of cancer, conditioned by its early diagnosis which is a challenging task for clinicians and dermatologists. In this regard, CAD systems based on machine learning and image processing techniques are developed to differentiate melanoma lesions from benign and dysplastic nevi using dermoscopic images. Generally, these frameworks are composed of sequential processes: pre-processing, segmentation, and classification. This architecture faces mainly two challenges: (i) each process is complex with the need to tune a set of parameters, and is specific to a given dataset; (ii) the performance of each process depends on the previous one, and the errors are accumulated throughout the framework. In this paper, we propose a framework for melanoma classification based on sparse coding which does not rely on any pre-processing or lesion segmentation. Our framework uses Random Forests classifier and sparse representation of three features: SIFT, Hue and Opponent angle histograms, and RGB intensities. The experiments are carried out on the public $PH^2$ dataset using a 10-fold cross-validation. The results show that SIFT sparse-coded feature achieves the highest performance with sensitivity and specificity of 100% and 90.3% respectively, with a dictionary size of 800 atoms and a sparsity level of 2. Furthermore, the descriptor based on RGB intensities achieves similar results with sensitivity and specificity of 100% and 71.3%, respectively for a smaller dictionary size of 100 atoms. In conclusion, dictionary learning techniques encode strong structures of dermoscopic images and provide discriminant descriptors.

**Keywords:** Melanoma, Classification, Sparse coding, Random forests, Dermoscopy

## 1. INTRODUCTION

Despite the fact that malignant melanoma only accounts for nearly 2% of all skin cancer cases, the vast majority of skin cancer deaths are due to malignant melanoma. According to the World Health Organisation, during the past decades, the incidence of this pathology has increased up to 132,000 diagnosed cases of melanoma.[1] The American Cancer Society estimated that during 2014 there would be 76,100 diagnosed new cases of melanoma, leading to death in 9710 cases .[2] At advanced stage, melanoma is incurable and the patients should go through surgery, possibly immunotherapy, chemotherapy, and/or radiation therapy. However, if diagnosed at its early stage, melanoma is the most treatable kind of cancer.[2,3] Indeed the patient survival rate has well increased, in the past decades, thanks to early diagnosis and treatment of melanoma in its early stages.

A well established criteria for early stage melanoma prognosis is the "ABCDE" rule[4] illustrated in fig. 1. This criteria is meant for a human reader to visually inspect an image of a skin lesion, and characterize this lesion based on the following visual cues:

(A) **A**symetry of the lesion

(B) irregularity of the lesion **B**orders

Further author information: (Send correspondence to M.R. or G.L)
M.R.: E-mail: mojdeh.rastgo-dastjerdi@u-bourgogne.fr
G.L.: E-mail: guillaume.lemaitre@u-bourgogne.fr

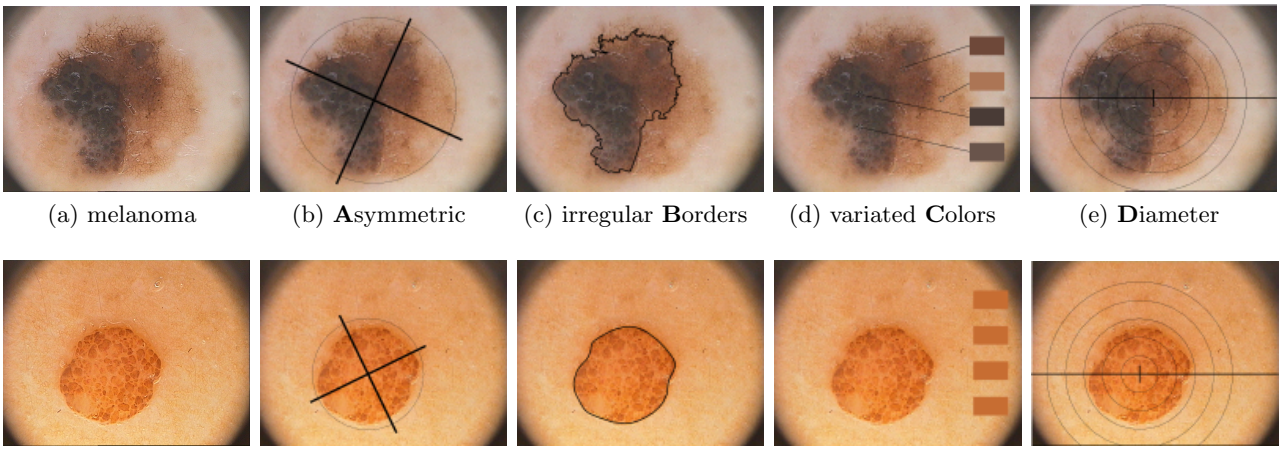

(a) melanoma (b) **A**symmetric (c) irregular **B**orders (d) variated **C**olors (e) **D**iameter

(f) benign lesion (g) non-**A**symmetric (h) regular **B**orders (i) unique **C**olor (j) **D**iameter

Figure 1: **A**BCD-lexicon comparison of two lesions. The top row corresponds to melanoma while the bottom row is a benign lesion.

(C) presence of variegated **C**olors within the lesion

(D) lesion size, evaluating if the **D**iameter of the lesion is greater than 6 mm

(E) evaluation of the lesion **E**volution over time, through regular screening.

Despite the aforesaid positive impact of these methodologies, visual inspection of medical images for diagnosis is prone to errors. Manning *et al.* state that the diagnosis error rates are comparable to the error rates found in any other human visual inspection task .[5] Thus, double readings and Computer-Aided Diagnosis (CAD) systems are placed to aid dermatologists and clinicians to mitigate this weakness. A variety of CAD systems are proposed that take advantage of image processing and Machine Learning to mimic the criteria defined by the "ABCDE" rule.[6] A prevalent schema for such CAD systems, consists of: image pre-processing to facilitate any subsequent task; segmentation to determine the extension of the lesion (emulating the reading of the image by a human grader); feature extraction to characterize the lesion; and further, classification of these features to drive the decision. To describe the lesions using highly cognitive terms such as lesion asymmetry or boundary regularity, requires accurate delineation of the lesions. For the clinicians case, finding this delineation is intrinsic to the visual inspection. However, for the case of CAD systems, the delineation is subject to the process of segmentation, which remains an open research topic.[7]

In this paper, we propose a more general framework which does not need pre-processing and segmentation of the lesions and is based on sparse coded features and Random Forests (RF) classifier[8] to detect melanoma in dermoscopic images.

The rest of this paper is organized as follows: an overview of related work is presented in Sect. 2. The proposed method is discuss in Sect. 3 while the experiment and obtained results are presented in Sect. 4 and 5, respectively. Finally the paper is concluded in Sect. 6.

## 2. RELATED WORK

In the past decade, numerous approaches have been proposed for automated recognition of melanoma lesions. The developed methods are commonly based on clinical or dermoscopy modality. These methods follow the usual classification framework of computer vision and consists of four common steps: (i) pre-processing, (ii) segmentation, (iii) feature extraction, and (iv) classification. Korotkov *et al.*[9] summarizes these methods and their properties. Unfortunately a fair comparison among the state of the art presented methods is not possible due to lack of the benchmark and common datasets.[6,9] Nevertheless recently a public dataset ( $PH^2$ ) has been

Table 1: Summary of the proposed classification methods using $PH^2$ dataset.

| Ref | Segmentation | features | Classification | | Balancing | Validation | Best performance | |
|---|---|---|---|---|---|---|---|---|
| | | | Classifier | Representation | | | SE | SP |
| Ruela *et al.*[13] | ✓ | Shape, FD[1] | AdB | - | ROS | OvA[1] | 92 | 74 |
| Ruela *et al.*[14] | ✓ | Color statistics | k-NN, AdB | - | ROS | OvA | 96 | 83 |
| Barata *et al.*[11] | ✓ | Opponent histogram gradients | AdB, SVM k-NN | BoW - | ROS | 10-fold[2] OvA | 100 | 75 |
| Barata *et al.*[17] | ✓ | Opponent histogram | k-NN | BoW | ROS | 10-fold | 98 | 86 |
| Abuzaghleh *et al.*[15] | ✓ | FFT2, DCT2 | SVM | - | - | - | 97.7 | - |
| Rastgoo *et al.*[16] | ✓ | Shape, color statistics opponent angle and Hue histogram CLBP, GLCM, HoG, Gabor[3] | - | RF LC[3] | DOS | OvA | 94 | 92 |

[1] Fourier descriptor (FD), One versus all (OvA).
[1] k-fold corss validation.
[2] Completed Local Binary Pattern (CLBP), Gray-Level Co-occurrence Matrix (GLCM), Histogram of Gradients (HoG), Learner combination (LC).

resealed for research purposes, thanks to Mendoncca *et al.*,.[10] Section 4 presents a detailed description of this dataset.

Subsequently, we emphasize on the most recent methods which are evaluated using this dataset. Table 1 summarizes these methods.

Barata *et al.*,[11,12] and ruela *et al.*[13,14] used different subsets of $PH^2$ dataset in their works.[10] Ruela *et al.*[13,14] compared the role of shape and colors for detection of melanoma vs. benign and dysplastic lesions using AdaBoost (AdB) classifier. Concerning the same problem, Barata *et al.*[11] proposed to use bag of words (BoW) representation of colors and gradient features. They compared different classifiers, such as AdB, kernel Support Vector Machine (SVM), and k-nearest-neighbor (NN). Their proposed algorithm achieved the highest Sensitivity (SE) and Specificity (SP) of 100% and 75%, respectively, when BoW representation with k-NN classifier was used. The authors, later used a similar scheme (BoW representation, k-NN classifier, and histogram of opponent color space histogram) to compare the effects of manual and automatic segmentation in the classification process. The results indicate that manual outperformed the automatic segmentation Classification frameworks using manual segmentation outperformed the automatic (SE and SP of 98% and 86%, respectively). Feature space, random over-sampling (ROS) was used in all the aforementioned methods to tackle the imbalance problem. To tackle the imbalance problem, feature space ROS was used in all the aforementioned methods.

Abuzaghleh *et al.*[15] also used $PH^2$ dataset. In this study the authors proposed automated recognition system based on color and shape features such as 2-D Fast Fourier Transform features (FFT2), Discrete Cosine Transform features (DCT2), size and complexity features. The authors proposed two classification approach: (i) multi-class and (ii) two-level classification. In both approaches SVM classifier was used. In later approach, in the first level, normal and abnormal lesions were classified, while in the second level, the abnormal lesions were divided into melanoma and dysplastic lesions. In later approach, the first level classifies normal and abnormal lesions while the second level works only with the abnormally classified lesions and differentiate melanoma and dysplastic nevi.

In our previous work, using the same dataset, we compared the effects of various colors, shape and texture features and ensemble approaches.[16] In this work the features were extracted from the segmented area and data space over-sampling (DOS) was used instead of ROS.[16] Using RF ensemble and combination of color and texture features the SE and SP of 94% and 92%, was achieved, respectively.

## 3. METHODOLOGY

As mentioned in the Sect. 1, the proposed framework, in comparison to previous methods (see Table 1), do not rely on pre-processing an segmentation and focus only on feature detection, extraction and classification. Figure 2 illustrates our proposed framework.

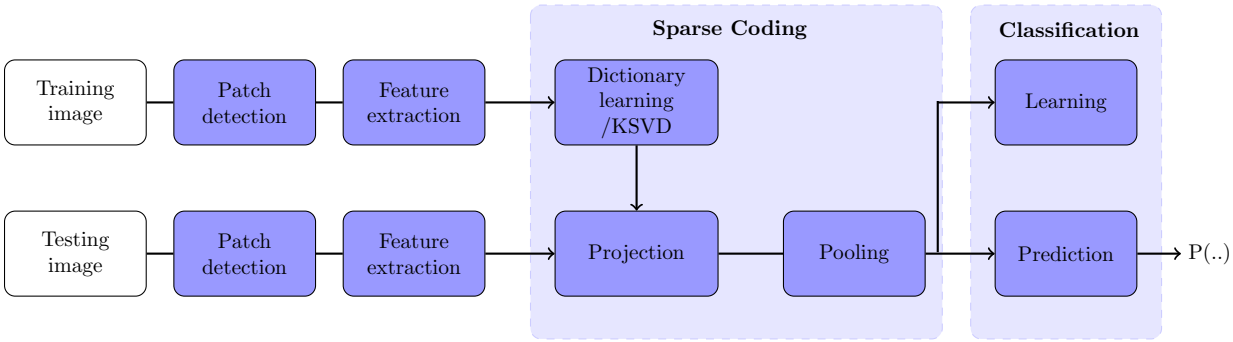

Figure 2: The proposed framework.

## 3.1 Feature extraction

### 3.1.1 Low-level features

In clinical environment, the prognosis of early stage melanoma relies upon visual cues, represented by a set of rules such as "ABCDE". One of the main characteristic is variegated colors and difference of color representation between melanoma and benign lesions. Textural difference, irregular and sharp borders are another valuable and distinguishable tool. In this study, three low-level features in line with the previous two discriminative criteria are used. Color variation criteria is described through two descriptors: opponent color space angle and hue histogram ($C_1$) and R,G,B intensities ($C_2$). While the texture, gradient and irregular borders is characterized via Scale-Invariant Feature Transform (SIFT) descriptor. These descriptors are presented into details in the remainder of this section. Furthermore, these features are locally extracted by partitioning the dermoscopic images into patches.

**Dense Scale-Invariant Feature Transform (SIFT)** descriptors are used to encode the local gradient information using an histogram-based representation.[18] SIFT descriptors are extracted over a regular grid such that each grid point is fixed at the center of each image patch. Typically, a region around the center is divided into $4 \times 4$ sub-regions from which a 8-bins histogram of the gradient orientations weighted by the gradient magnitudes is computed. Finally, these histograms are concatenated to build the final descriptor with a final size of 128 dimensions. The SIFT implementation used in this work is provided by Vedaldi *et al.*[19]

**The opponent color space angle and hue histogram (*C1*)** have been first proposed by Van de Weijer and Schmidt as local color features.[20] These descriptors are robust to photometric variations (i.e., shadow, shading, specularities, and light source changes) as well as geometrical variations (i.e, viewpoint, zoom, and object orientation). The hue ($H_{\mathcal{O}}$) and angle ($\theta_{\mathcal{O}}$) of opponent color space ($\mathcal{O}_{1,2,3}$) are formulated as shown in Eq. 2 and Eq. 3, respectively. The opponent color space transformation is defined as in Eq. 1.

$$\begin{pmatrix} \mathcal{O}_1 \\ \mathcal{O}_2 \\ \mathcal{O}_3 \end{pmatrix} = \begin{pmatrix} (R-G)/\sqrt{2} \\ (R+G-2B)/\sqrt{6} \\ (R+G+B)/\sqrt{3} \end{pmatrix} , \tag{1}$$

$$H^{\mathcal{O}} = \arctan\left(\frac{\sqrt{3}(R-G)}{R+G-2B}\right) , \tag{2}$$

$$\theta_d^{\mathcal{O}} = \arctan\left(\frac{\sqrt{3}(R'_d-G'_d)}{R'_d+G'_d-2B'_d}\right) , \tag{3}$$

where $d$ denotes the spatial coordinates of $(x,y)$ and $R'_d$, $G'_d$, $B'_d$ denote the first order derivatives of $RGB$ with respect to the coordinates.

This color descriptor is built by taking a 42 bins histogram for the opponent angle $\theta_d^{\mathcal{O}}$ and the hue channel $H^{\mathcal{O}}$, for a final descriptor size of 84 dimensions.

**The color intensities (*C2*)** represent the color information in a simplest form, their intensities. This descriptor concatenates the color intensities $R$, $G$ and $B$ to create the feature descriptor.

### 3.1.2 High-level features

High-level descriptor is computed using sparse coding techniques. Sparse signal representation has become very popular in the past decades and lead to state-of-the-art results in various applications such as face recognition,[21] image denoising, image inpainting,[22] and image classification.[23] The main goal of sparse modeling is to efficiently represent the images as linear combination of a few typical patterns, called atoms, selected from the dictionary. Here, we intend to use sparse representation of the low-level extracted features for melanoma classification. Sparse coding consists of three main steps: (i) dictionary learning, (ii) low-level features projection, and (iii) feature pooling[24] (as illustrated in Fig. 2).

**Sparse approximation** Given a dictionary $\mathbf{D} \in \mathbb{R}^{n \times K}$ composed of $K$ atoms and an original signal $\mathbf{y} \in \mathbb{R}^n$ (i.e., one feature vector), the sparse approximation corresponds to find the sparest vector $\mathbf{x} \in \mathbb{R}^K$ such that:

$$\arg\min_{\mathbf{x}} \|\mathbf{y} - \mathbf{D}\mathbf{x}\|_2 \qquad \text{s.t. } \|\mathbf{x}\|_0 \leq \lambda \tag{4}$$

where $\lambda$ is a specified sparsity level.

Solving the above optimization problem is an NP-hard problem.[25] However, approximate solutions are obtained using greedy algorithms such as Matching Pursuit[26] or Orthogonal Matching Pursuit (OMP).[27,28] We used the batch-OMP variant which offers a more efficient algorithm than the standard OMP for our specific problem.[24]

**Dictionary learning** As stated previously, the sparse approximation is computed given a specific dictionary $\mathbf{D}$, which involves a learning stage from a set of training data. This dictionary is learned using $K$-SVD which is a generalized version of $K$-means clustering and uses Singular Value Decomposition (SVD). The dictionary is built, by iteratively solving the optimization problem of Eq. 5, by alternatively computing the sparse approximation of $\mathbf{X}$ and the dictionary $\mathbf{D}$.

$$\arg\min_{\mathbf{D},\mathbf{X}} \|\mathbf{Y} - \mathbf{D}\mathbf{X}\|_2 \qquad \text{s.t. } \|\mathbf{x}_i\|_1 \leq \lambda \tag{5}$$

where $\mathbf{Y}$ is a training set of low-level descriptors, $\mathbf{X}$ is the associated sparse coded matrix (i.e., set of high-level descriptors) with a sparsity level $\lambda$, and $\mathbf{D}$ is the dictionary with $K$ atoms.

Given $\mathbf{D}$, $\mathbf{X}$ is computed using the batch-OMP algorithm, while given $\mathbf{X}$, $\mathbf{D}$ is sequentially updated, one atom at a time using SVD.

**Low-level features projection** Once the dictionary is learned, each set of low-level features $\mathbf{F}_I \in \mathbb{R}^{n \times p}$ extracted from $p$ patches in an image is encoded using the dictionary $\mathbf{D}$, solving the optimization problem presented in Eq. 4 such that $\mathbf{F}_I \simeq \mathbf{D}\mathbf{X}_I$.

**Feature pooling** The sparse coded matrix $\mathbf{X}_I$ is max-pooled to build a final descriptor $\mathbf{f}$ characterizing the given image, such that:

$$\mathbf{f}_i = \max_j \left( |\mathbf{X}_I(i,j)| \right), \ \forall i = 1, \cdots, K \ . \tag{6}$$

Figure 3 illustrate the training and testing stage, using sparse coded features.

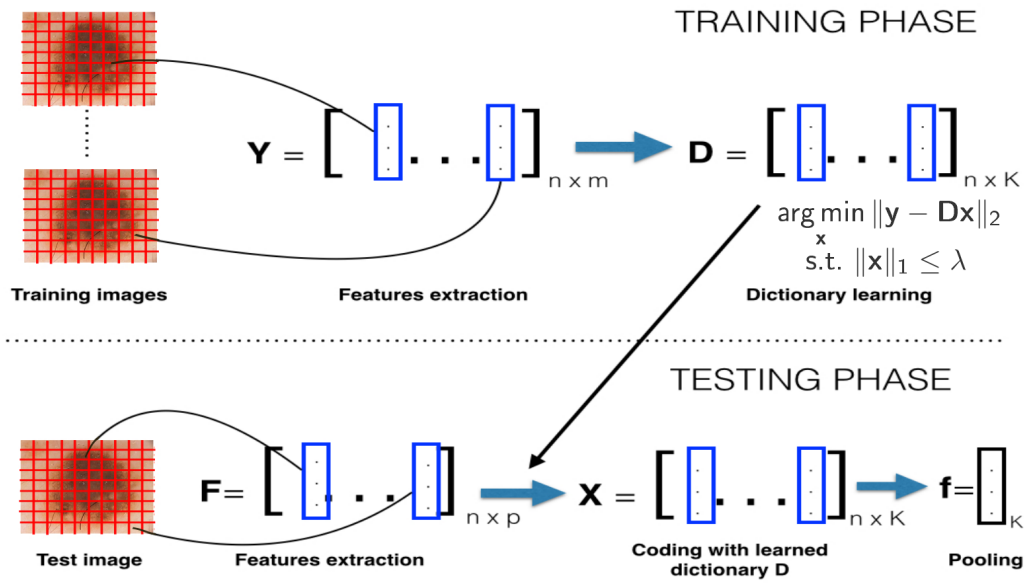


Figure 3: Sparse coded representation for training and testing samples.

### 3.2 Feature classification

#### 3.2.1 Over-sampling from imbalanced dataset

Similarly to Barata *et al.*,[11] the imbalanced issue of the dataset is tackled by over-sampling the samples of the minority class. New samples are generated to get a balanced set by randomly repeating original samples of the minority class with an additional Gaussian noise $\mathcal{N}(0, 0.0001)$.

#### 3.2.2 Random Forests (RF)

The classification is performed using a RF classifier. RF is an ensemble of decision trees[8] which generalizes the classification process by applying two types of randomization: at the tree level, each tree is fed by a bootstrap made of $S'$ samples built from the original data of size $S$ such that $S = S'$, and at the node level, a subset of feature dimensions $m$ is randomly selected from the original dimension $M$ such that $m = \sqrt{M}$. The trees in RF are grown to their maximum length without any pruning. Each tree in the ensemble casts a unit vote in the final prediction and the final prediction is based on combination of all the votes. RF is used with 1000 un-pruned trees using gini criterion and the original feature dimension.

## 4. EXPERIMENTS

The experiments are conducted on the public $PH^2$ dataset. This dataset was acquired at *Dermatology Service of Hospital Pedro Hispano, Matosinhos, Portugal*[10] with Tuebinger Mole Analyzer system with a magnification of 20×. The 8-bits RGB color dermoscopic images were obtained under the same conditions with a resolution of 768 px × 560 px. This dataset contains 200 dermoscopic images divided into 80 benign, 80 dysplastic and 40 melanoma lesions. The lesions are segmented and their histological diagnosis are provided as ground-truth.

In our experiments seven images are discarded due to artefacts such as hair occlusions. Thus, they are conducted on a subset of the dataset consisting of 39 melanoma, 78 benign, and 76 dysplastic lesions. The patch size used to extract the feature is 10 px × 10 px. The three low-level features are sparsely encoded considering three sparsity levels $\lambda = \{2, 4, 8\}$ and different number of atoms $K = \{100, 200, \cdots, 1000\}$. The classification is performed in a 10-fold cross-validation model in which 80% of the data is used for training and 20% for testing.

Table 2: The obtained results with different number of atoms and sparsity levels. The first, second, and third highest results for each sparsity level are highlighted in different shades of gray from dark to light color, respectively.

| Features | Color1 | | | | | | Color2 | | | | | | SIFT | | | | | |
|---|---|---|---|---|---|---|---|---|---|---|---|---|---|---|---|---|---|---|
| Sparsity level | 2 | | 4 | | 8 | | 2 | | 4 | | 8 | | 2 | | 4 | | 8 | |
| Dictionary size | SE | SP | SE | SP | SE | SP | SE | SP | SE | SP | SE | SP | SE | SP | SE | SP | SE | SP |
| 100 | 65.6 | 49.6 | 51.5 | 49.4 | 41.4 | 59.7 | 100 | 71.7 | 48.5 | 71.3 | 59.9 | 60 | 1.4 | 99.4 | 0 | 100 | 1.4 | 99.7 |
| 200 | 50.1 | 59.3 | 52.7 | 53.5 | 51.5 | 50 | 57.2 | 64 | 95.8 | 86.6 | 71.4 | 72 | 65.6 | 47.5 | 34.3 | 78 | 20 | 95 |
| 300 | 59.8 | 65.4 | 52.8 | 71 | 57.1 | 62.3 | 30 | 80 | 65.7 | 75.4 | 85.7 | 85.6 | 58.6 | 47.7 | 64.3 | 51.1 | 8.6 | 88.7 |
| 400 | 67 | 78.6 | 62.6 | 81.3 | 69.9 | 76 | 38.5 | 66 | 85.8 | 77.3 | 78.6 | 91.4 | 62.8 | 74.6 | 59.9 | 64.7 | 71.3 | 58.2 |
| 500 | 78.7 | 79 | 71.4 | 78.3 | 51.3 | 84 | 54.2 | 59.7 | 61.4 | 69.6 | 82.9 | 83.4 | 58.5 | 92 | 61.2 | 72.9 | 54 | 56.7 |
| 600 | 98.6 | 82.5 | 68.7 | 89.6 | 64 | 89.9 | 48.7 | 78.4 | 50 | 64.6 | 91.4 | 89.3 | 85.8 | 86.6 | 61.4 | 73.3 | 51.3 | 53.4 |
| 700 | 92.8 | 89.9 | 72.8 | 91.9 | 54.4 | 95.9 | 37.1 | 75.4 | 72.8 | 72 | 80 | 82.6 | 98.6 | 84.6 | 73 | 94.8 | 47 | 62.4 |
| 800 | 92.9 | 81.4 | 100 | 88.4 | 78.5 | 89.7 | 40 | 70.9 | 58.6 | 80.1 | 97.2 | 83.9 | 100 | 90.3 | 97.1 | 93 | 48.5 | 72.7 |
| 900 | 90 | 88 | 80 | 92 | 79.9 | 95.4 | 25.7 | 81.3 | 19.9 | 91.1 | 95.7 | 73.1 | 95.7 | 81.8 | 80 | 94.5 | 54.2 | 78.5 |
| 1000 | 100 | 86.8 | 80 | 89.6 | 94.3 | 91.7 | 34.3 | 70.7 | 42.7 | 76.5 | 100 | 73.8 | 90 | 83.5 | 71.4 | 89.8 | 51.3 | 90.3 |

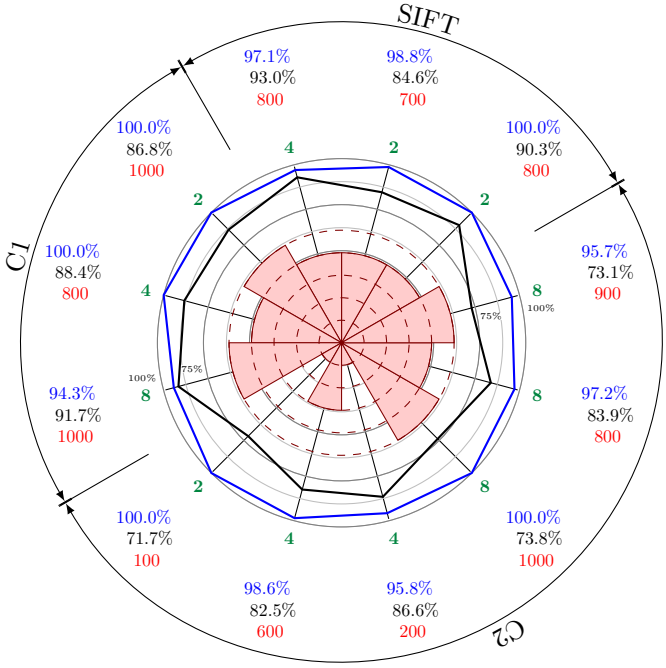


Figure 4: The 12 highest result achieved by RF classifier and sparse representation of SIFT, *color1*, and *color2* features with different **sparsity levels** are illustrated in blue and black as sensitivity and specificity, respectively, while their dictionary size is represented in red. A comparison of the dictionary sizes is also presented in middle of the graph, which contains five levels with maximum dictionary sizes of 1000, 800, 600, 400, 200 for each level respectively.

## 5. RESULTS

The results of the experiment are shown in terms of SE and SP in Table 2. The highest classification rate in respect of each feature type and each sparsity level are highlighted in different shades of gray from dark to light. The results show that *C1* and SIFT sparse coded features perform better with sparsity levels of 2 and 4, respectively, while *C2* performs better with sparsity level of 8. In general, larger dictionary sizes lead to better

classification performance, independently to the feature type and the sparsity level. More precisely, dictionaries with more than 600 atoms are preferable. Figure 4 illustrate the 12 best results. Although, SIFT and *C1* sparse coded features achieve the best classification performance in comparison with *C2*, it can be noted that *C2* features represent the dermoscopic images in their simplest form and create comparable results.

## 6. CONCLUSION AND FUTURE WORK

In this work, we proposed a novel classification framework of melanoma lesions, based on sparse representation of the low-level features. Our framework does not need the primary steps of pre-processing and segmentation of the lesions and provide more general algorithm to solve this problem. We proposed to use a well-known color descriptor based on Hue and angel histograms of opponent color space, and SIFT as a texture descriptor. We also consider to represent the images in their simplest form and consider the second color descriptor as R,G and B intensities. An extensive comparison based on different dictionary sizes and several sparsity levels were carried out on the $PH^2$ dataset. The results highlighted the advantage of the proposed method where an RF classifier and a sparse representation of SIFT features with a dictionary size of 800 and sparsity level of 2 achieved the highest performance (SE and SP of 100% and 90.3%, respectively). In general, the obtained results outperform the state of the art. As avenues for future research, a comparison of sparse learned dictionary with Bag-of-Word models can be performed.

## REFERENCES


1. "World health organization, skin cancer."
2. A. C. Society, "Cancer facts & figures 2014," 2014.
3. A. Forsea, V. Del Marmol, E. de Vries, E. Bailey, and A. Geller, "Melanoma incidence and mortality in europe: new estimates, persistent disparities," *British Journal of Dermatology* **167**(5), pp. 1124–1130, 2012.
4. N. R. Abbasi, H. M. Shaw, *et al.*, "Early diagnosis of cutaneous melanoma: revisiting the abcd criteria," *Jama* **292**(22), pp. 2771–2776, 2004.
5. D. Manning, A. Gale, and E. Krupinski, "Perception research in medical imaging," *The British journal of radiology* , 2014.
6. M. Rastgoo, R. Garcia, O. Morel, and F. Marzani, "Automatic differentiation of melanoma from dysplastic nevi," *Computerized Medical Imaging and Graphics* **43**, pp. 44–52, 2015.
7. J. S. Duncan and N. Ayache, "Medical image analysis: Progress over two decades and the challenges ahead," *Pattern Analysis and Machine Intelligence, IEEE Transactions on* **22**(1), pp. 85–106, 2000.
8. L. Breiman, "Random forests," *Machine learning* **45**(1), pp. 5–32, 2001.
9. K. Korotkov and R. Garcia, "Computerized analysis of pigmented skin lesions: a review," *Artificial intelligence in medicine* **56**(2), pp. 69–90, 2012.
10. T. Mendonça, P. M. Ferreira, J. S. Marques, A. R. Marcal, and J. Rozeira, "Ph 2-a dermoscopic image database for research and benchmarking," in *Engineering in Medicine and Biology Society (EMBC), 2013 35th Annual International Conference of the IEEE*, pp. 5437–5440, IEEE, 2013.
11. C. Barata, M. Ruela, M. Francisco, T. Mendona, and J. Marques, "Two systems for the detection of melanomas in dermoscopy images using texture and color features," *IEEE Systems Journal,* **8**, pp. 965–979, Sept 2014.
12. C. Barata, J. S. Marques, and J. Rozeira, "The role of keypoint sampling on the classification of melanomas in dermoscopy images using bag-of-features," in *Pattern Recognition and Image Analysis*, pp. 715–723, Springer, 2013.
13. M. Ruela, C. Barata, T. Mendonca, and J. S. Marques, "On the role of shape in the detection of melanomas," in *8th International Symposium onImage and Signal Processing and Analysis (ISPA)*, pp. 268–273, IEEE, 2013.
14. M. Ruela, C. Barata, and J. S. Marques, "What is the role of color symmetry in the detection of melanomas?," in *Advances in Visual Computing*, pp. 1–10, Springer, 2013.
15. O. Abuzaghleh, B. D. Barkana, and M. Faezipour, "Automated skin lesion analysis based on color and shape geometry feature set for melanoma early detection and prevention," in *Systems, Applications and Technology Conference (LISAT), 2014 IEEE Long Island*, pp. 1–6, IEEE, 2014.

16. M. Rastgoo, O. Morel, F. Marzani, and R. Garcia, "Ensemble approach for differentiation of malignant melanoma," in *The International Conference on Quality Control by Artificial Vision 2015*, pp. 953415–953415, International Society for Optics and Photonics, 2015.
17. C. Barata, J. S. Marques, and M. E. Celebi, "Towards an automatic bag-of-features model for the classification of dermoscopy images: The influence of segmentation," in *8th International Symposium on Image and Signal Processing and Analysis (ISPA)*, pp. 274–279, IEEE, 2013.
18. D. G. Lowe, "Object recognition from local scale-invariant features," in *Computer vision, 1999. The proceedings of the seventh IEEE international conference on*, **2**, pp. 1150–1157, Ieee, 1999.
19. A. Vedaldi and B. Fulkerson, "Vlfeat: An open and portable library of computer vision algorithms," in *Proceedings of the international conference on Multimedia*, pp. 1469–1472, ACM, 2010.
20. J. Van De Weijer and C. Schmid, "Coloring local feature extraction," in *Computer Vision–ECCV 2006*, pp. 334–348, Springer, 2006.
21. J. Wright, A. Y. Yang, A. Ganesh, S. S. Sastry, and Y. Ma, "Robust face recognition via sparse representation," *Pattern Analysis and Machine Intelligence, IEEE Transactions on* **31**(2), pp. 210–227, 2009.
22. M. Elad and M. Aharon, "Image denoising via sparse and redundant representations over learned dictionaries," *Image Processing, IEEE Transactions on* **15**(12), pp. 3736–3745, 2006.
23. D. Sidibé, I. Sadek, and F. Mériaudeau, "Discrimination of retinal images containing bright lesions using sparse coded features and svm," *Computers in biology and medicine* **62**, pp. 175–184, 2015.
24. R. Rubinstein, M. Zibulevsky, and M. Elad, "Efficient implementation of the k-svd algorithm using batch orthogonal matching pursuit," *CS Technion* **40**(8), pp. 1–15, 2008.
25. M. Elad, *Sparse and Redundant Representations: From Theory to Applications in Signal and Image Processing*, Springer Publishing Company, Incorporated, 1st ed., 2010.
26. S. G. Mallat and Z. Zhang, "Matching pursuits with time-frequency dictionaries," *Signal Processing, IEEE Transactions on* **41**(12), pp. 3397–3415, 1993.
27. Y. C. Pati, R. Rezaiifar, and P. Krishnaprasad, "Orthogonal matching pursuit: Recursive function approximation with applications to wavelet decomposition," in *Signals, Systems and Computers, 1993. 1993 Conference Record of The Twenty-Seventh Asilomar Conference on*, pp. 40–44, IEEE, 1993.
28. G. Davis, S. Mallat, and M. Avellaneda, "Adaptive greedy approximations," *Constructive approximation* **13**(1), pp. 57–98, 1997.